Characterization of Electrosynthesized Polydihaloanilines

M. A. del Valle,[1] F. R. Díaz,[1] J. L. Torres,[1] P. P. Zamora,[1] M. A. Godoy,[2] J. C. Bernède[3]

[1]*Laboratorio de Polímeros, Facultad de Química, Pontificia Universidad Católica de Chile, Vicuña Mackenna 4860, Santiago, Chile*
[2]*Facultad Ciencias de la Salud, Universidad Diego Portales, Ejercito 141, Santiago, Chile*
[3]*Laboratoire des Matériaux photovoltaïques (LAMP), Equipes d' Accueil (EA) 3829, Faculté des Sciences et dês Techniques, Universite de Nantes Atlantique, 2 Rue de la Houssieniere, BP 992098, Nantes, France F-44000*

Received 19 September 2008; accepted 16 May 2009
DOI 10.1002/app.31063
Published online 27 August 2009 in Wiley InterScience (www.interscience.wiley.com).

ABSTRACT: The nucleation and growth mechanism of some homopolymers of aniline (six monomers were studied: 3,5-dichloroaniline, 2,5-dichloroaniline, 2,6-dichloroaniline, 2,3-dichloroaniline, 2,5-dibromoaniline, and 2,6-dibromoaniline), synthesized by potentiostatic methods, was determined with a mathematical model that considers different contributions from current–time transients with a gold-disc electrode. Deconvolution of the transients for the dichlorinated monomers showed $IN3D_{ct}$ and $PN3D_{dif}$ contributions (where $IN3D_{ct}$ refers to an instantaneous nucleation and three-dimensional growth mechanism under charge-transfer control and $PN3D_{dif}$ refers to a progressive nucleation and three-dimensional growth mechanism under diffusion control), whereas IN2D and $PN3D_{dif}$ components and IN2D, $IN3D_{ct}$, and $PN3D_{dif}$ components (where IN2D refers to an instantaneous nucleation and two-dimensional growth mechanism) were needed for 2,5-dibromoaniline and 2,6-dibromoaniline, respectively. The percentage of the contribution of the current–time transient to the total charge was worked out for each monomer. The effect of the scan rate on the voltammetric profile during the potentiodynamic electrosynthesis of the polymers was studied too. Curves of the current versus the square root of the potential scan rate were recorded for a selected group of monomers, and the slope was considered an estimation of the diffusion coefficient of the respective monomer. Furthermore, the electrosynthesized polymers were characterized with Fourier transform infrared, ultraviolet–visible, X-ray photoelectron spectroscopy, and scanning electron microscopy. Microanalysis, used to establish the ratio of the atomic percentages of P and N for each polymer synthesized at a constant potential, was performed for doped and undoped polymers. This parameter was a measure of the degree of electrochemical doping. The conductivity of the doped and undoped polymers was also measured. Hence, the systematic characterization of this analogue series of monomers allows, before generalization, an adequate experimental design to prepare polymers with the properties required for their use. J Appl Polym Sci 115: 107–115, 2010

Key words: conducting polymers; electrochemistry; nucleation

INTRODUCTION

Conductive polymers have been synthesized by electrochemical means for about 30 years. The synthesis of conjugated polymers, the study of doping–undoping processes, and the application of polymers in a variety of fields account for the development of electrochemical methods applied to the synthesis of conducting polymers. Electropolymerization offers some advantages over chemical methods; for example, the polymer can be obtained in its doped, conductive form, and the degree of doping can be controlled in an efficient and simple way. Besides, in some applications and characterizations, the polymer deposited onto the electrode can be used directly without any further modification. From a theoretical standpoint, the technique offers the advantage of gathering a great deal of simultaneous information during the electropolymerization process. The technique itself becomes a powerful tool for characterization because information can be inferred about the nature of the process occurring during the electropolymerization. Kinetic and thermodynamic parameters that may help to characterize the conducting polymer can be determined as well. Furthermore, electrochemistry allows studying and understanding the systems in which the conductive polymers will be used. Finally, electrochemistry is a powerful tool for studying and understanding the nucleation and growth mechanism (NGM) that renders polymeric films.[1–4] An NGM study is a complex matter even for the formation of metallic deposits on metals (electrocrystallization) because a series of factors must be considered.[5–8] Accordingly, models have been developed that permit us to establish the nucleation kinetics and kind of growth during

Correspondence to: M. A. del Valle (mdvalle@uc.cl).
Contract grant sponsor: Fondo Nacional de Desarrollo Científico y Tecnológico; contract grant numbers: 1050953, 1095156.

electrocrystallization.[9] It is noteworthy that a difference exists when the deposit on the metallic substrate is a polymer: the nature of the film and the mechanism through which this is generated are different. Asavapriyanont et al.[10] were the first to study the polymerization of pyrrol and *N*-methylpyrrol by electrochemical means. An analysis of the current–time (*j–t*) transient of the initial state led them to conclude that, under the experimental conditions employed, the process fits an instantaneous nucleation model with three-dimensional growth. Bade et al.[11] studied the nucleation and growth process of polyaniline (PANI) on Au and Pt microelectrodes. In this article, we report the determination of the NGM of some homopolymers derived from aniline obtained by electropolymerization at a controlled potential. To this end, a mathematical model and deconvolution of the *j–t* transients were used.

In an earlier investigation, we reported chemical polymerization.[12–15] Considering that electrochemistry is fundamental to the study of conducting polymers, in this case we have set forth a thorough analysis that depends on the electrochemical perturbation (potentiostatic or potentiodynamic). This analysis is also complemented by other techniques to add to the knowledge of the phenomenon that must be contemplated when this tool is used, which fundamental to obtaining, characterizing, and controlling the properties of the material to be prepared.

Cyclic voltammetry was used to study the effect of the scan rate on the voltammetric profile during the electrosynthesis of the polymers, and curves of j versus the square root of the potential scan rate ($v^{1/2}$) were recorded for four selected monomers. The resulting polymers were also characterized with Fourier transform infrared (FTIR), ultraviolet–visible (UV–vis), scanning electron microscopy (SEM), and X-ray photoelectron spectroscopy (XPS). Microanalysis of the polymers to establish the level of electrochemical doping and conductivity measurements were performed too.

EXPERIMENTAL

Dihalogenated monomers derived from aniline were purchased from Aldrich (St. Louis, MO) and were purified from a methanol/water mixture before use. All the other reagents were also from Aldrich but were used as received. Electrosynthesis and electrochemical characterization were performed on an Autolab PGP 201 (Utrecht, The Netherlands) potentiostat/galvanostat or a PGSTAT 20 with a three-compartment, three-electrode cell and a CH_3CN/H_2O (60/40 v/v) mixture as the solvent. The concentrations of the monomer and supporting electrolyte [tetraethylammonium hexafluorophosphate ($TEAPF_6$)] used throughout this work were 0.03 and 0.1 mol/L, respectively. A gold disc (0.07-cm^2 geometric area) was used to study the NGM and the potentiostatic and potentiodynamic characterization. A gold sheet (2-cm^2 geometric area) was used for preparing large amounts of the polymers to be characterized by other techniques. Tin oxide (SnO_2), plated on glass (conducting glass; 0.5-cm^2 geometric area), was also employed in the electrochemical characterization of the polymers, whereas a 2-cm^2 electrode was used for characterization by other techniques. All potentials quoted in this article refer to a Ag/AgCl electrode in tetraethylammonium chloride to match the potential of the saturated calomel electrode (SCE) at room temperature.[16] The counter electrode was a Pt coil. All voltammetric studies as well as the synthesis with the potentiodynamic technique were performed at a scan rate of 100 mV/s. The electrolytic solutions were purged with high-purity argon before and during the measurement. Microanalysis was performed on a JEOL (Peabody, MA) JMS-5800 LV scanning microscope. A JEOL 6400F scanning microscope was employed for obtaining SEM images. XPS spectra were recorded on a Leybold (SPECTRO Analytical Instruments GmbH, Kleve, Germany) LHS-12 spectrometer at the University of Nantes/Centre National de la Recherche Scientifique (Nantes, France). FTIR spectra were measured on a Brucker (Michigan City, IN) Vector 22 spectrophotometer with KBr pellets. UV–vis spectra were recorded on a Shimadzu (Tokyo, Japan) UV-3101 PC spectrophotometer in 1-cm cells. Conductivity measurements were carried out at room temperature on pellets of the polymer (24,000 psi) by the four-probe method on an Elchema (Potts-dam, NY) CM 508 electrometer.

RESULTS AND DISCUSSION

To facilitate the discussion, the monomers were separated into two groups. The first includes the dibrominated derivatives of aniline [2,5-dibromoaniline (2,5-DiBr) and 2,6-dibromoaniline (2,6-DiBr)], and the second includes the dichlorinated derivatives [2,5-dichloroaniline (2,5-DiCl), 2,6-dichloroaniline (2,6-DiCl), 3,5-dichloroaniline (3,5-DiCl), and 2,3-dichloroaniline (2,3-DiCl)].

The best fit for the experimental curves corresponds to the following general equation:

$$j = at[\exp(-bt^2)] + c[1 - \exp(-dt^2)] + et^{-0.5}[1 - \exp(-ft^2)] \quad (1)$$

In this equation, all terms represent contributions described in the literature.[6,7] The first and second terms correspond to instantaneous nucleation

TABLE I
Parameters *a*, *b*, *c*, *d*, *e*, and *f* for Each Monomer

Monomer	E (V)	a (mA cm^{-2} s^{-1})	b (s)	c (mA/cm^2)	d (s)	e (mA cm^2 s^1)	f (s^{-2})
3,5-DCl	1.497	–	–	0.00028	0.0217	0.15519	0.00005
2,5-DCl	1.475	–	–	0.17091	0.0002	0.06635	0.00150
2,6-DCl	1.470	–	–	0.59109	0.00022	0.27676	0.00180
2,3-DCl	1.460	–	–	0.00646	0.00212	0.34651	0.00007
2-SS	1.460	–	–	0.89464	0.00003	–	–
2,5-DBr	1.380	0.00255	0.00123	0.01625	1.48×10^{-6}	–	–
2,6-DBr	1.270	0.00069	0.00046	0.14082	0.00012	0.37412	0.00012

The parameters were estimated from the models employed for the deconvolution of the *j*–*t* transients with eq. (1). E = electrode potential.

mechanisms under charge-transfer control with two-dimensional (IN2Dct) and three-dimensional (IN3Dct) growth, respectively. The last term corresponds to a progressive nucleation and three-dimensional growth mechanism under diffusion control ($PN3D_{dif}$). The constants a, b, c, d, e, and f can be described as follows:

$$a = \frac{2\pi nMhFN_{2D}k_2^2}{\rho}, \quad b = \frac{\pi N_{2D}M^2k_2^2}{\rho^2} \tag{2}$$

$$c = NFk_3', \quad d = \frac{\pi N_{3D}M^2k_3^2}{\rho^2} \tag{3}$$

$$e = \frac{\pi FD^{0.5}C_\infty}{\rho^{0.5}}, \quad f = \frac{A'k\pi D}{2} \tag{4}$$

where F, M, and ρ are the Faraday constant, molecular weight, and density of the deposited polymer, respectively. N_{2D} and N_{3D} are the instantaneous numbers of nuclei formed at $t = 0$ in two- and three-dimensional forms, respectively. k_2 is the growth rate constant of the two-dimensional nucleus. k_3 and k_3' are the rate constants of the three-dimensional nucleus for parallel and perpendicular growth, respectively. D, C_∞, n, and h are the diffusion coefficient, bulk concentration, number of electrons, and nucleus height, respectively. Finally, A' and k in eq. (4) are defined by eqs. (5) and (6):

$$A' = AN_{dif} \tag{5}$$

$$k = \frac{4}{3}\left(\frac{8\pi C_\infty M}{\rho}\right)^{0.5} \tag{6}$$

where A is the rate constant of nucleus formation and N_{dif} is the number of nuclei formed at $t = 0$ under diffusion control. The values of the constants in eq. (1) for each monomer, evaluated from the variables involved in each contribution, are summarized in Table I.

It is important to point out that the only experimental variable considered in this research was the nature of the monomer because all transients were determined under the same experimental conditions mentioned earlier.

On the basis of the experimental results, the deconvolution of the *j*–*t* transient of the respective monomer afforded the following NGM.

First, for dichlorinated aniline monomers, contributions of the $IN3D_{ct}$ and $PN3D_{dif}$ types were obtained; that is, in eq. (1), the first term is zero. Figure 1 shows typical chronoamperograms for the electropolymerization of 3,5-DiCl and 2,5-DiCl obtained by the working electrode potential being stepped to 1.470 and 1.497 V, respectively. The model for the best fit and the individual contributions are also depicted in Figure 1. *j*–*t* transients for the other dichlorinated derivatives obey the same mechanism, but for each monomer, the weight of each contribution will be different. Table II lists the percentage contribution to the global model of each investigated monomer. For poly(3,5-DiCl) and poly(2,3,-DiCl), both components contribute to the mechanism in a very short time, whereas for $t >$ 10 s, the $IN3D_{ct}$ component becomes negligible, and $PN3D_{dif}$ predominates. As for poly(2,5-DiCl) and poly(2,6-DiCl), a mixed behavior has been observed: for $t <$ 40 s, the $PN3D_{dif}$ component prevails over $IN3D_{ct}$, whereas at long times, the $IN3D_{ct}$ component becomes more important.

Because the morphology of the polymers depends on the NGM, a morphology made up of three-dimensional nuclei of various sizes is expected for the polymers derived from dichlorinated monomers on the basis of the mechanism to which the experimental data have been fitted.

Second, the model used for deconvolution of the *j*–*t* transient of the 2,5-DiBr monomer is formed by IN2D and $PN3D_{dif}$ contributions; that is, in eq. (1), the middle term is zero. Figure 2 depicts the experimental transient, the model to which it fits, and the individual contributions. In addition, Figure 2 shows that for $t <$ 40 s, the IN2D contribution predominates over the $PN3D_{dif}$ contribution, whereas for $t >$

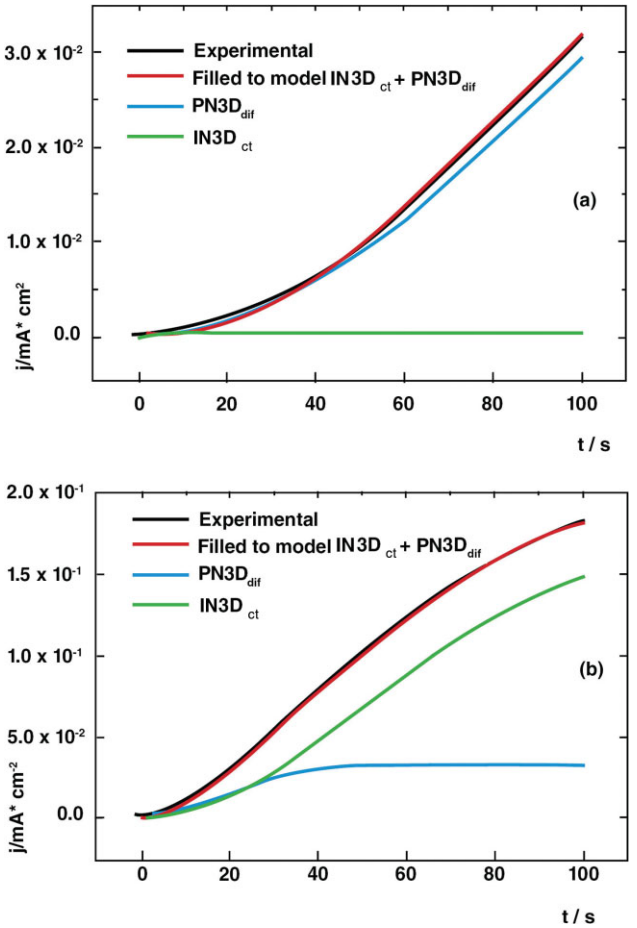

Figure 1 *j–t* transients for the electropolymerization of (a) 3,5-DiCl (electrode potential = 1.470 V; interface = Au/0.037*M* monomer + 074*M* $TEAPF_6$; H_2O/CH_3CN = 60/40 v/v) and (b) 2,5-DiCl (electrode potential = 1.497 V; interface = Au/0.037*M* monomer + 074*M* $TEAPF_6$; H_2O/CH_3CN = 60/40 v/v). [Color figure can be viewed in the online issue, which is available at www.interscience.wiley.com.]

50 s, the latter becomes much more important. From a morphological point of view, this transient is related to a system in which many nuclei are formed in the beginning that grow in a homogeneous and compact way, on top of which three-dimensional nuclei of different sizes grow further.

TABLE II
Contribution of Each *j–t* Transient to the Overall Charge

Monomer	IN2D (%)	$IN3D_{ct}$ (%)	$PN3D_{dif}$ (%)
3,5-DCl	–	9.6	90.4
2,5-DCl	–	72.3	27.7
2,6-DCl	–	69.5	30.5
2,3-DCl	–	15.1	83.9
2-SS	–	100	–
2,5-DBr	89.9	–	10.1
2,6-DBr	4.9	40.8	54.3

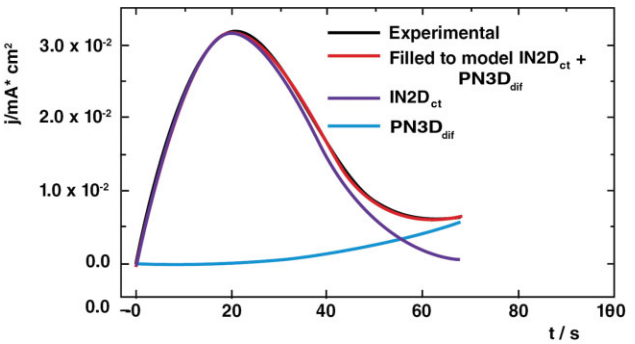

Figure 2 *j–t* transient for the electropolymerization of 2,5-DiBr. The experimental conditions are the same as those in Figure 1, except for the theoretical model (IN2D + $PN3D_{dif}$) and electrode potential (1.460 V). [Color figure can be viewed in the online issue, which is available at www.interscience.wiley.com.]

Third, the model used for deconvolution of the *j–t* transient of 2,6-DiBr involves three components: IN2D, $IN3D_{ct}$, and $PN3D_{dif}$. Figure 3 depicts the experimental transient, the fitted curve, and the individual components that describe the model. From Figure 3, it can be seen that for $t < 10$ s, IN2D prevails, but for longer times, this component becomes less significant, and $IN3D_{ct}$ and $PN3D_{dif}$ become more important. According to this model, a morphology in which small nuclei coexist with large ones can be expected.

Effect of the scan rate potential on the voltammetric profile in the electrosynthesis of the polymers

For the purpose of obtaining additional information regarding the electropolymerization process, the influence of v on the previously studied processes occurring during the potentiodynamic electropolymerization of the monomers was investigated.

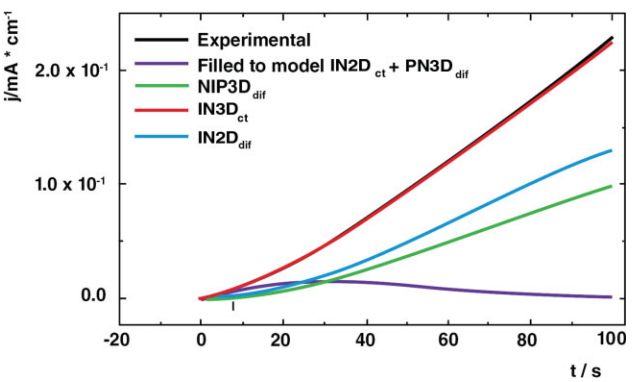

Figure 3 *j–t* transient for the electropolymerization of 2,6-DiBr. The experimental conditions are the same as those in Figure 1, except for the theoretical model (IN2D + $IN3D_{ct}$ + $PN3D_{dif}$) and electrode potential (1.460 V). [Color figure can be viewed in the online issue, which is available at www.interscience.wiley.com.]

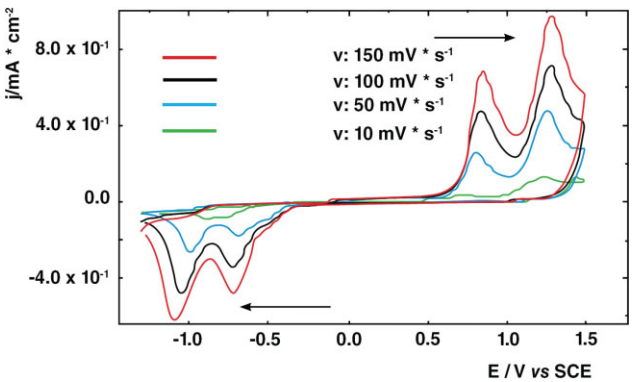

Figure 4 Electro-oxidation of 2,5-DiBr with cyclic voltammetry at different v values (E = electrode potential; interface = Au/0.037M monomer + 0.074M $TEAPF_6$; H_2O/CH_3CN = 60/40; cycle number = 60). [Color figure can be viewed in the online issue, which is available at www.interscience.wiley.com.]

Figure 4 shows, as an example, cycle number 60 for the electropolymerization of 2,5-DiBr at four scan rates. The other monomers presented similar behavior.

These voltammograms show a current increase with an increasing scan rate, and this is consistent with classical electrochemistry predictions. In addition, no new signals can be observed in these voltammograms, and this indicates that both redox processes are the same. As the scan rate increases, the anodic and cathodic peak potentials are shifted anodically and cathodically, respectively, by about 50 mV. Besides, the signal gets wider as the scan rate decreases, this being particularly evident for v = 10 mV/s, and this is an indication of the irreversible nature of these processes.[17] The same behavior has been obtained, though to a lesser extent, for PANI.[18] On the other hand, at 10 mV/s, the distinctive loop of nucleation and growth[5,19,20] can be observed, shifting to smaller values as the scan rate decreases. The amplitudes of both peaks in the respective voltammograms are similar, pointing to processes with charge-transfer rates very close to one another.

The electropolymerization process is quite complex because it involves chemical and electrochemical components.[21] In terms of classical electrochemistry, this means that we are dealing with a so-called dirty process in which the laws valid in classical electrochemistry are sometimes not necessarily valid for the electropolymerization process. Consequently, it seems awkward to talk about electropolymerization conducted under diffusion control because in practice it has been demonstrated that the actual process is more complex. An example of this is the concept of a working electrode in electropolymerization: at the onset of electrolysis, a series of very complex, simultaneous processes occur on the working electrode that invalidate the use of the classical equations for electrochemical processes. After some time, the electrode is modified, and the initial characteristics are lost. Now we have a modified electrode, that is, an electrode coated with a polymer or oligomers on which a polymeric film is growing. In this second step, the process may meet the laws of classical electrochemistry, which initially are not valid, because a new state has been reached that can be considered stationary. To check this statement, a correlation was sought between j of the second oxidization process of the monomers and $v^{1/2}$ because it is well known that if a linear relationship exists, the process is diffusion-controlled.[20] Figure 5 depicts j–$v^{1/2}$ curves for currents of cycles 3, 31, and 60 (selected to consider three different stages of the electropolymerization) at scan rates of 10, 50, 100, and 150 mV/s. The straight line corresponding to cycle 3, assigned to the initial stage, presents the worst correlation coefficient, whereas this coefficient improves for cycle 31, and for cycle 60, the regression coefficient is quite good. These results confirm the hypothesis that in certain cases, after some time, the electropolymerization process follows the laws of classical electrochemistry.

In this investigation, analogous behavior was observed for the six monomers, demonstrating that, after a given period of time, all the electropolymerization processes became diffusion-controlled.

Finally, additional information can be obtained from Figure 5. The peak current (j_p) is related to $v^{1/2}$ with the following equation:

$$j_p = K\, D_O^{1/2}\, v^{1/2} \tag{7}$$

where D_O is the diffusion coefficient of the oxidized form and K is a constant involving parameters such as the concentration, working electrode area, and reversibility coefficient. These parameters are equal, or at least similar, for all the investigated monomers; therefore, the slope of the j_p–$v^{1/2}$ lines can be considered an estimation of the diffusion coefficient of the respective monomer. Because of the nature of the electropolymerization, it is not possible to predict whether the diffusion is from the bulk of the solution to the electrode surface or to a determinate site in the polymeric film. Also, there is no guarantee that the deposit on the electrode is fully homogeneous. Therefore, values of the slope are an estimation of the diffusion coefficient of each monomer. These are relative values and are useful only for comparison; that is, they cannot be considered absolute values of the diffusion coefficients. Table III shows the slopes of the j_p–$v^{1/2}$ lines and the regression coefficients of the four monomers, which displayed a linear behavior (the criterion employed for linearity was a regression coefficient >98%). For the other three monomers, the regression coefficient ranged

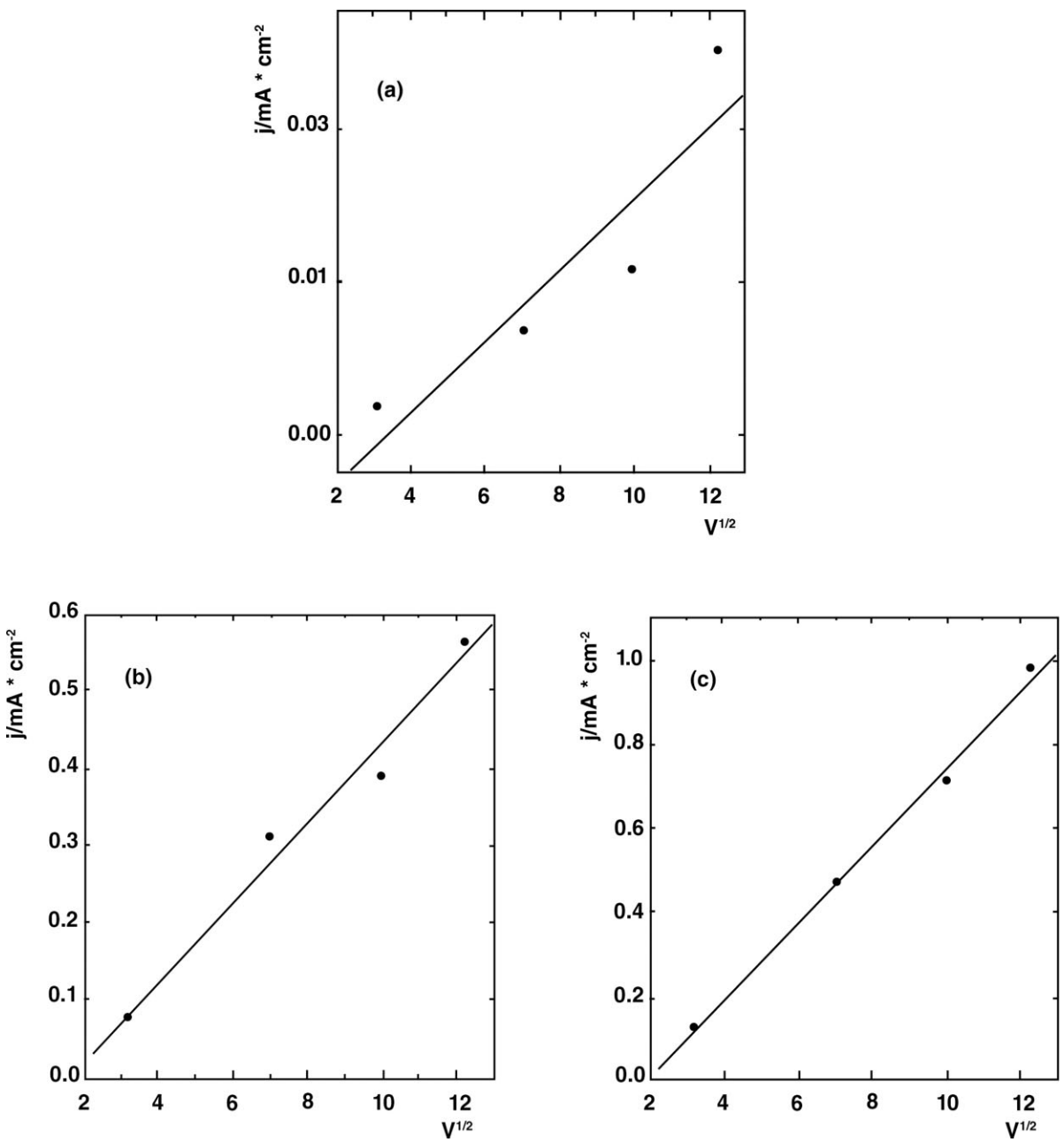

Figure 5 j_p–$v^{1/2}$ relationship for 2,5-DiBr (interface = Au/0.037*M* 2,5-DiBr + 0.074*M* $TEAPF_6$; H_2O/CH_3CN = 60/40 v/v): (a) cycle 3, (b) cycle 30, and (c) cycle 60.

from 90 to 92%. As for monomers with a regression coefficient less than 98%, a likely explanation for the low values is that the time needed to reach linearity is longer than that corresponding to the 60 cycles employed in this work. In Table III, the values of the slope for the dibrominated monomers are quite close to one another, and so are those corresponding to the dichlorinated derivatives. These results may be considered evidence that the process is valid for analyzing the trend among analogous species. Finally, the values of the slope in Table III also show that the diffusion coefficients of dichlorinated monomers are higher than those of dibrominated monomers. This difference can be attributed to a higher mobility, which is mainly associated with the lower mass of the dichlorinated monomers.

TABLE III
Slope (*m*) and Linear Regression Coefficient (*R*) of the j–$v^{1/2}$ Curves

Monomer	*m*	*R*
2,5-DBr	0.09218	0.99761
2,6-DBr	0.07806	0.98274
2,3-DCl	0.18672	0.98943
2,5-DCl	0.18970	0.99725

Characterization of the potentiostatically synthesized homopolymers by FTIR, UV–vis, XPS, electron-probe microanalysis, conductivity, and SEM

A summary of the main results obtained from the characterization of the polymers synthesized at a constant potential is presented next.

FTIR and UV–vis spectroscopy

The main features of the FTIR studies are as follows. All the spectra for the compounds synthesized on Au and conductive glass (CG) are alike; that is, no structural differences exist between polymers deposited onto Au and CG. Besides, this behavior is common to all the studied polymers. Polymers electrochemically and chemically obtained show the same FTIR main bands; that is, the polymeric structures are the same, no matter what synthetic procedure is used.

The ratio of the C=C band intensities, corresponding to the benzenoid–diamine (I_B) and quinoid–diimine (I_Q) units, affords information about the redox state of the polymers. On the basis of the values of the I_Q/I_B ratio, it can be stated that the polymers are in their polyemeraldine state.

All UV–vis spectra for electrosynthesized dihalogenated polymers in the base form deposited onto Au and CG are similar. Spectra on both Au and CG display the same three bands at 260, 315, and 510 nm. A hypsochromic shift (related to a steric effect) can be observed when these bands are compared to those of PANI (300 and 500 nm). In addition, chemically synthesized dihalogenated polymers show the same three bands, and this demonstrates the analogousness of the structures of their polymeric chains.

XPS

The C1s deconvoluted spectrum for undoped Poly(2,5-dichloroaniline) [P(2,5 DC1)] synthesized on Au shows four contributions at 286.66, 286.3, 287.46, and 288.53 eV. The last signal, attributable to a C—O bond, is due to atmospheric contamination, the solvent, and the supporting electrolyte. The Cl2p spectrum displays the typical bands of an aromatic C—Cl bond: a doublet at 201.71 and 203.51 eV. XPS spectra for undoped P(2,5-DC) electropolymerized on CG show no significant qualitative differences from those for undoped P(2,5-DC) deposited onto Au, except for a small variation in the signal position; that is, the two polymers are structurally similar. The N1s spectrum is the most important because it provides information about the oxidation state of the polymer and allows a comparison of the results with those obtained by FTIR spectroscopy. Dihalogenated polymers synthesized on Au and CG present two kinds of N1s spectra. P(2,5-DC) synthesized on Au can be used as a example. The N1s spectrum splits into two signals, affording information about the redox state of the polymer. The ratio of the area of the signal attributable to the amine group (A_a) and the area corresponding to the imine group (A_i) is an estimation of the redox state of the polymer. The A_a/A_i ratio for P(2,5-DiCl) synthesized at a constant potential on Au was 1.084, and this indicated the emeraldine conducting state of the polymer.

Electron-probe microanalysis

The P/N atomic percentage ratios for each polymer, doped [$(P/N)_d$] and undoped [$(P/N)_u$], synthesized at a constant potential on Au were determined. This parameter is a measure of the degree of electrochemical doping of the polymer. From the data obtained, the following conclusions have been drawn. First, electrochemical synthesis has greatly improved the level of doping of the surveyed polymers in comparison with those obtained by chemical means with inorganic acids as dopants.[14] Second, there is no significant difference in the degree of doping when the synthesis is performed potentiostatically or potentiodynamically on Au; that is, $(P/N)_d$ is independent of the electrochemical method of choice. Third, for all the studied polymers, the level of doping is always greater on Au than on CG. This finding may be related to the higher potentials used for the synthesis and doping of the polymers on Au.

Conductivity

The conductivity of doped and undoped polymers synthesized at a constant potential on Au was measured at 20°C. A difference of up to 5 orders of magnitude was observed for dichlorinated compounds, demonstrating the efficiency of the electrochemical doping. The lowest conductivity values were found for dibrominated polymers. The conductivity of the doped polymers lies in an intermediate position between those of conducting and insulating polymers (Table IV).

Another observation is the great difference between the conductivities of the electrochemically and chemically synthesized polymers, and this is directly related to the efficiency of the electrochemical doping. Also, no significant difference was observed for the conductivity of a polymer synthesized on Au at a constant potential and the same polymer obtained with cyclic voltammetry. Finally, all polymers electrosynthesized on Au presented higher conductivities than the same polymers deposited onto CG. This is a result of the higher level of doping of the compounds synthesized on Au.

TABLE IV
Conductivity

Monomer	Conductivity (S/cm)	
	Doped	Undoped
3,5-DCl	1.25×10^{-12}	15.20×10^{-7}
2,5-DCl	2.30×10^{-12}	21.20×10^{-7}
2,6-DCl	2.10×10^{-12}	12.60×10^{-7}
2,3-DCl	1.20×10^{-12}	19.50×10^{-7}
2,5-DBr	0.85×10^{-12}	5.60×10^{-9}
2,6-DBr	12.10×10^{-10}	20.20×10^{-7}

SEM

SEM micrographs of polymers potentiostatically synthesized on Au in their doped state are shown in Figure 6. In general, three-dimensional granules predominate, producing a cauliflower-like surface. The differences observed among the micrographs lie only in the granule size and in its distribution.

As previously found, three-dimensional growth of the deposited polymers predominated for longer times of electrolysis and should agree with the observed morphology. On the other hand, from the deduced NGM model, a certain correlation exists between the granule size and distribution, which would validate the method for predicting the morphology of a polymeric deposit. Particularly for dibrominated polymers in which, in addition to the three-dimensional contribution, a two-dimensional component exists, the surface of the deposited polymer exhibits more compact zones as a result of the two-dimensional growth. The differences in the morphology among the dichlorinated polymers lie in the granule size and the distribution of the same in agreement with NGM predictions; that is, predominance of the PN3D contribution gives rise to larger granules.

CONCLUSIONS

The nucleation and growth model, which permits deconvoluting the respective *j–t* transients, is strongly dependent on the monomeric structure and is composed of one or more contributions that,

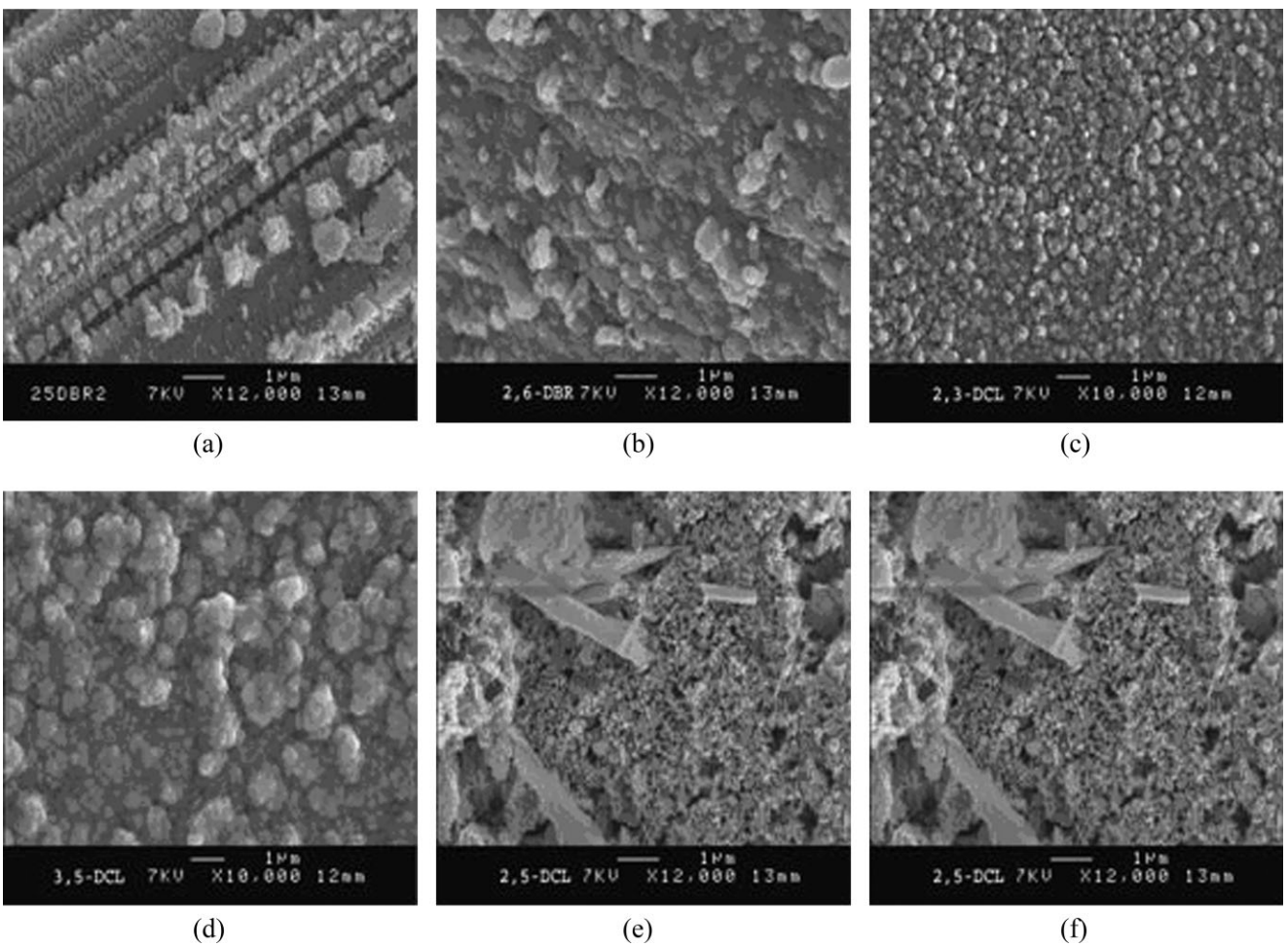

Figure 6 SEM micrographs of polymers synthesized at a constant potential: (a) P(2,5-DiBr) (electrode potential = 1.46 V), (b) P(2,6-DiBr) (electrode potential = 1.46 V), (c) P(2,3-DiCl) (electrode potential = 1.38 V), (d) P(3,5-DiCl) (electrode potential = 1.47 V), (e) P(2,5-DiCl) (electrode potential = 1.497 V), and (f) P(2,6-DiCl) (electrode potential = 1.475 V).

simultaneously or successively, contribute to the total charge. The predominance of one or another contribution to the global NGM is determined by the electrolysis time, and for longer periods of time, the main contribution is always diffusion-controlled. A correlation between the NGM and the morphology of the obtained deposit has been established, validating the model; simultaneously, it is also an adequate tool for predicting and controlling the type of morphology that is required.

The potentiodynamic method of electrosynthesis has revealed that the redox processes of the studied derivatives are analogous to those reported for PANI. This fact has been corroborated by XPS studies.

The study of the effect of the scan rate on the electropolymerization process has indicated that above a certain number of cycles, the oxidation of the monomer is diffusion-controlled. At shorter times of electrolysis or with a smaller number of cycles, the morphology of the deposit noticeably depends on the type of electrochemical perturbation. For longer times or with a higher number of cycles (>60), the morphology of the deposit becomes independent of the kind of electrochemical perturbation. Nevertheless, the structure of the homopolymers obtained by electrochemical techniques is similar to that of the homopolymers obtained by chemical methods. All the electropolymerized homopolymers were obtained in their intermediate redox state, emeraldine, which corresponds to the more conducting form in this class of polymers. The level of doping of the electrochemically prepared polymers is always higher than that found for the same polymers obtained by chemical methods. Besides, the level of doping is slightly higher for dichlorinated polymers than for dibrominated polymers. The conductivity and solubility of the electrochemically synthesized homopolymers derived from aniline are always greater than those of the same compounds chemically prepared. Finally, it is possible to increase the conductivity of the polymers derived from aniline with electrochemical methods of synthesis.

Thus, this investigation enables the selection of the monomer of this series and the respective working conditions on the basis of the properties required for the electronic device (e.g., higher or lower conductivity and morphology).

References

1. Simonet, J.; Raoult-Berthelot, J. Prog Solid State Chem 1991, 1, 90.
2. Sied, A. A.; Dinesan, M. K. Talanta 1991, 38, 815.
3. González-Tejera, M. J.; Carrillo, I.; Hernández-Fuentes, I. Electrochim Acta 2000, 45, 1973.
4. Hwang, B. J.; Santhanam, R.; Wu, C. R.; Tsai, Y. W. J Solid State Electrochem 2001, 5, 280.
5. Córdoba, R.; del Valle, M. A.; Arratia, A.; Gómez, H.; Schrebler, R. J Electroanal Chem 1994, 377, 75.
6. Schrebler, R.; Cury, P.; del Valle, M. A. Electrochim Acta 2002, 48, 397.
7. Koryta, J.; Dvorak, J.; Kavan, L. Principles of Electrochemistry; Wiley: New York, 1993.
8. del Valle, M. A.; Ugalde, L.; Diaz, F. R.; Bodini, M. E.; Bernède, J. C.; Chaillou, A. Polym Bull 2003, 51, 55.
9. Fleischman, M.; Thirsk, H. R. In Advances in Electrochemistry and Electrochemical Engineering; Delahay, P., Ed.; Wiley: New York, 1963; p 123.
10. Asavapriyanont, S.; Chandler, G. K.; Gunawardena, G.; Pletcher, D. J Electroanal Chem 1984, 177, 229.
11. Bade, K.; Isakova, V.; Schultze, J. W. Electrochim Acta 1992, 37, 2255.
12. Diaz, F. R.; Sánchez, C. O.; del Valle, M. A.; Tagle, L. H.; Bernède, J. C.; Tregouet, Y. Synth Met 1998, 92, 99.
13. Diaz, F. R.; del Valle, M. A.; Sánchez, C. O.; Ugalde, L.; Gargallo, L. Synth Met 1999, 101, 161.
14. Diaz, F. R.; Sánchez, C. O.; del Valle, M. A.; Radic, D.; Bernède, J. C.; Tregouet, Y.; Moliniè, P. Synth Met 2000, 110, 71.
15. Diaz, F. R.; Sánchez, C. O.; del Valle, M. A.; Torres, J. L.; Tagle, L. H. Synth Met 2001, 118, 25.
16. East, G. A.; del Valle, M. A. J Chem Educ 2000, 77, 97.
17. Bard, A. J.; Faulkner, L. R. Electrochemical Methods, Fundamentals and Applications; Wiley: New York, 1980.
18. Pruneaunu, S.; Veress, E.; Marian, I.; Oniciu, I. J Appl Polym Sci 1999, 34, 2733.
19. Hillman, A. R.; Mallen, A. F. J Electroanal Chem 1987, 220, 351.
20. Scharifker, B.; García, E.; Marino, W. J Electroanal Chem 1991, 300, 85.
21. del Valle, M. A.; Diaz, F. R.; Bodini, M. E.; Alfonso, G.; Soto, G. M.; Borrego, E. Polym Int 2005, 54, 526.